

57-30-90

Copy
RM L57E14a

262

NACA RM L57E14a

8777

7728
JUN 24 1957

0144812

TECH LIBRARY KAFB, NM

NACA

RESEARCH MEMORANDUM

p 2 3 3

AERODYNAMIC HEATING AND BOUNDARY-LAYER TRANSITION ON A
1/10-POWER NOSE SHAPE IN FREE FLIGHT AT MACH NUMBERS

UP TO 6.7 AND FREE-STREAM REYNOLDS NUMBERS

UP TO 16×10^6

By Benjamin J. Garland, Andrew G. Swanson, and
Katherine C. Speegle

Langley Aeronautical Laboratory
Langley Field, Va.

TECH
RL 2231

Classification changed to *UNCLASSIFIED*
By Authority of *NASA-52, 17 Aug 61 - TAB 10 1961*
(OFFICER AUTHORIZED TO CHANGE)

By *N. G. Speegle*
NAME AND

GRADE OF OFFICER MAKING CHANGE
23 FEB 57

This material contains information affecting the National Defense of the United States within the meaning of the espionage laws, Title 18, U.S.C., Secs. 793 and 794, the transmission or revelation of which in any manner to an unauthorized person is prohibited by law.

NATIONAL ADVISORY COMMITTEE FOR AERONAUTICS

WASHINGTON

June 17, 1957

HADC ADJ '57 - 4403

•

•

•

•



•

•



0144812

NATIONAL ADVISORY COMMITTEE FOR AERONAUTICS

RESEARCH MEMORANDUM

AERODYNAMIC HEATING AND BOUNDARY-LAYER TRANSITION ON A
1/10-POWER NOSE SHAPE IN FREE FLIGHT AT MACH NUMBERS
UP TO 6.7 AND FREE-STREAM REYNOLDS NUMBERS
UP TO 16×10^6

By Benjamin J. Garland, Andrew G. Swanson, and
Katherine C. Speegle

SUMMARY

A modified 1/10-power nose shape has been tested in free flight at Mach numbers up to 6.7 and free-stream Reynolds numbers based on diameter up to 16×10^6 . Measured heating rates were presented and compared with calculated values. Agreement ranges from poor on the forward portion of the nose to good on the rearward portion.

The local Reynolds numbers of transition based on calculated momentum thickness varied between 1,600 and 350. Laminar flow was maintained at momentum thickness Reynolds numbers of about 1,000 until the free-stream Reynolds number based on a length of 1 foot reached about 27×10^6 . At slightly higher free-stream Reynolds numbers transition occurred at momentum thickness Reynolds numbers as low as 250.

INTRODUCTION

The National Advisory Committee for Aeronautics is conducting flight tests to determine the heat-transfer characteristics of various blunt nose shapes. References 1 to 4 present results of some of these tests in the Mach number range from 2 to 5 at high Reynolds numbers.

Recently a new rocket system has been developed for blunt nose shapes which is capable of reaching a Mach number of 7 at altitudes under 15,000 feet. This system allows testing at extremely high Reynolds numbers and heating rates. The two-stage system employs an M5 JATO booster and a "Recruit" sustainer rocket motor (JATO, 1.52-KS-33,550, XML9). The Recruit motor used in the investigation reported herein was made available by the U. S. Air Force.

This report presents results from the first research test employing this system. The test nose shape was a modified 1/10-power shape of 6-inch diameter. Heat-transfer and transition data were obtained at Mach numbers up to 6.7 and Reynolds numbers based on diameter up to 16×10^6 . The flight test was conducted at the Langley Pilotless Aircraft Research Station, Wallops Island, Va., in December 1956.

SYMBOLS

c_p	specific heat, Btu/slug-°F
D	diameter of nose, 0.5 ft
g	acceleration due to gravity, 32.2 ft/sec ²
J	mechanical equivalent of heat
M	Mach number
N_{Pr}	Prandtl number
N_{St}	Stanton number
p	pressure, lb/sq ft
β	rate of change of velocity at stagnation point, $\frac{dV_{t2}}{dx}$
q	heating rate, Btu/(sq ft)(sec)
R	Reynolds number
R_θ	local Reynolds number based on laminar boundary-layer momentum thickness
η_r	recovery factor
T	temperature
t	time, sec
V	velocity, ft/sec
x	distance along axis, in.

ρ	density, slugs/cu ft
S	surface distance from stagnation point, in.
r	distance from axis to surface of test nose, in.
r_B	base radius of test nose, 0.25 ft
γ	ratio of specific heats
τ	wall thickness, ft
h	heat-transfer coefficient, Btu/ft-sec- $^{\circ}$ F

Subscripts:

aw	adiabatic wall
t	stagnation
l	local conditions, just outside boundary layer
∞	free-stream conditions
i	inner surface
s	outer surface
w	pertaining to wall
T	transition
t_2	stagnation conditions behind normal shock
l	based on length of 1 foot

MODEL, INSTRUMENTATION, AND TEST

Model

The general model arrangement and pertinent dimensions are shown in figure 1. A photograph of the model is shown in figure 2. The model consisted of a "Recruit" rocket motor (JATO, 1.52-KS-33,550, XM19) with an instrumentation-carrying section mounted on the fore end of the motor.

~~CONFIDENTIAL~~

The test nose, whose shape was determined by the equation

$$\frac{r}{r_B} = 0.79750x^{1/10} + 0.020783x$$

was then mounted on the forward end of the instrumentation section. The model was stabilized by a magnesium flare of 10° half-angle.

The test nose was spun from Inconel and had a nominal thickness of 0.05 inch. The measured skin thicknesses at the temperature measuring points are presented in table I. A sketch of the nose showing thermocouple and pressure measuring locations is presented in figure 3. A photograph of the nose is shown in figure 4. The average surface roughness of the nose was 6 to 8 microinches with maximum surface roughness of 15 microinches. This finish was attained with No. 600 paper. It should be noted that this nose was not given the superpolished finish of the nose shapes reported in references 3 and 4.

The model was boosted by a fin-stabilized M5 JATO rocket motor. A photograph of the model and booster on the launcher is shown in figure 5.

Instrumentation

The model was equipped with six channels of telemetering. One channel transmitted temperatures, three transmitted pressures, and two transmitted accelerations (longitudinal and transverse). The temperature channel was commutated about every 0.1 second to transmit temperature measurements at the locations given in table I. The thermocouples were spotwelded to the inner surface of the skin. The maximum probable error of the temperature measurements was ±2 percent of the calibrated full-scale; or, in this case, ±40°. A more complete discussion of the general methods of the temperature telemetering techniques employed is presented in reference 5.

In addition to the instrumentation carried internally, the model was tracked by a CW Doppler velocimeter and an NACA modified SCR-584 radar set to provide the velocity of the model and trajectory data, respectively. Atmospheric and wind conditions were determined by means of a radiosonde launched near the time of flight and tracked by a Rawin set AN/GMD-1A.

Test

The model was launched at an elevation angle of 70°. The booster accelerated the model to a Mach number of about 3. The model and expended booster coasted upwards for a short predetermined time until the sustainer rocket ignited. At sustainer ignition the locking diaphragm which held the two stages together was broken or blown out and the model accelerated to a maximum Mach number of 7.

~~CONFIDENTIAL~~

Near peak Mach number the model went to an angle of attack for unknown reasons, resulting in extremely high heating rates on the windward side of the model. This heating, in conjunction with the airloads at angle of attack, probably caused the loss of telemeter signal which occurred shortly after burnout.

Data presented in this report are for the time of flight up to 5.6 seconds ($M = 6.7$) during which time the model was near zero angle of attack. The Mach number of 6.7 was reached at an altitude of 10,000 feet which corresponds to a Reynolds number of about 32×10^6 based on a length of 1 foot or 16×10^6 based on test nose diameter.

DATA REDUCTION

The following data were obtained as a function of flight time from ground radar, telemeter, and radiosonde:

- (1) Skin-temperature measurements (fig. 6)
- (2) Model velocity, Mach number, and altitude (fig. 7)
- (3) Air properties at any given time (fig. 8) - static pressure, density, and temperature

These data were reduced into heating rate for various flight conditions.

$$q = \rho_w c_{p,w} \tau_w \frac{dT_{w,av}}{dt}$$

The thickness τ_w was measured at each of the thermocouple locations and is listed in table I. The material density ρ_w is constant. The variation of specific heat with temperature is presented in reference 6. Since the temperature measurements were made on the inner surface of the skin $T_{w,i}$, it was necessary to calculate the outer surface $T_{w,s}$ by a method developed by P. R. Hill of the Langley Pilotless Aircraft Research Division. The mean temperature $T_{w,av}$ was estimated to be the average of the inner and outer skin temperatures. This average temperature was used to determine $\frac{dT_{w,av}}{dt}$.

Figure 9 presents the pressure distribution measured on a 1/10-power shape in the preflight jet of the Langley Pilotless Aircraft Research Division at Wallops Island, Va. The pressure ratios $p_l/p_{t,2}$ presented

are used invariant with Mach number. The pressures measured on the model in flight were not used because an insufficient number of measurements was made to give an adequate distribution and because the measured pressures appeared to be in error. For example, during the early part of the flight, the pressure measured by the first pickup was greater than the stagnation pressure behind a normal shock; this difference was greater than the maximum probable error.

CALCULATION OF HEATING RATE

Values of heating rate q for the conditions for which experimental data are presented were calculated from the following equation:

$$q = h(T_{aw} - T_{w,s}) \quad (1)$$

Heating Rates Over Forward Portion of Nose

The forward portion of the nose was considered to be that part having ratios of surface distance from stagnation point to base radius (s/r_B) of 0.416 to 0.908. Heating rates over the forward portion of the nose were calculated from the following form of equation (1):

$$q = \frac{h_l}{h_t} (T_{aw} - T_{w,s}) h_t \quad (2)$$

Equation (2) may also be written

$$q = \frac{h_l}{h_t} \left[\eta_r (T_t - T_l) + T_l - T_{w,s} \right] h_t \quad (3)$$

In order to calculate the value of q by equation (3), estimates were made of stagnation, surface, and local temperatures, recovery factor, stagnation heating rate, and ratio of local heating rate to stagnation heating rate.

Temperatures.— The stagnation temperature T_t was computed from the stagnation enthalpy given by the energy equation

$$V^2/2Jg = \int_{T_\infty}^{T_t} c_p dT$$

~~CONFIDENTIAL~~

which takes into account the variation of the specific heat of air with temperature.

The surface temperature $T_{w,s}$ was determined from the measured inner surface temperature $T_{w,i}$ by the method mentioned previously.

The local temperature just outside the boundary layer T_l was calculated by using the pressure distribution presented in figure 9, the normal-shock relations of reference 7, and the total temperature calculated previously.

Recovery factor.- The recovery factor η_r was assumed to be equal to the square root of the Prandtl number for laminar flow and equal to the cube root of the Prandtl number for turbulent flow. The Prandtl number was based on the surface temperature.

Stagnation heat-transfer coefficient.- The stagnation heat-transfer coefficient h_t is a function of the rate of change of velocity at the stagnation point. The value of the parameter $\beta D/V_\infty$, measured in the preflight jet at a Mach number of 2, was 0.47. For a hemisphere the value of this parameter for a Mach number of 2 is 1.44. Since the heat-transfer coefficient is a function of the square root of $\beta D/V_\infty$,

$$\frac{h_{t(1/10)}}{h_{t,h}} = \frac{(\sqrt{\beta D/V_\infty})_{1/10}}{(\sqrt{\beta D/V_\infty})_h} = \frac{\sqrt{0.47}}{\sqrt{1.44}} = 0.57$$

The value of h_t for the 1/10-power shape is then computed by using the theory of Sibulkin (ref. 8) for the stagnation heating on a hemisphere.

Ratio of heat-transfer coefficients.- The ratio of local heat-transfer coefficient to stagnation heat-transfer coefficient (h_l/h_t) was determined by the method of Stine and Wanlass (ref. 9), modified for the 1/10-power shape by using the pressure distribution given in figure 9. The variation of h_l/h_t around the nose is presented in figure 10. This distribution was used for all Mach numbers.

Heating Rates Over Rearward Portion of Nose

The rearward portion of the nose was considered to be that part having ratios of surface distance from the stagnation point to base radius (s/r_B) of 0.908 to 1.92. Heating rates over the rearward portion of the nose were calculated from equation (1) written in the following form:

~~CONFIDENTIAL~~

$$q = (N_{St} \rho V c_p)_l (T_{aw} - T_{w,s}) \quad (4)$$

Equation (4) may also be written

$$q = (N_{St} \rho V c_p)_l \left[\eta_r (T_t - T_l) + T_l - T_{w,s} \right] \quad (5)$$

For this calculation, stagnation, surface, and local temperatures and recovery factor were obtained in the same manner as for the forward portion of the nose. Density, specific heat, velocity, and Stanton number were calculated for use in equation (5).

Density, specific heat, and velocity.- The local conditions, density ρ , specific heat c_p , and velocity V , were calculated by using the Newtonian pressure distribution shown by the dashed curve in figure 9, the normal-shock relations of reference 7, and the total temperatures calculated previously.

Stanton numbers.- The Stanton numbers were obtained from the theories of Van Driest for laminar and turbulent flow (refs. 10 and 11, respectively). In both cases the Reynolds number was based on one-half the surface length from the stagnation point to the measuring station, according to the theory for cones.

RESULTS AND DISCUSSION

The experimental heating rates around the nose are presented in figure 11 together with values of heating rates calculated by the methods presented in the previous sections.

Transition

Figure 11 shows that laminar flow evidently existed over all the measuring stations only during the very early portion of the flight.

Figure 11(a) which presents data for a flight time of 2.2 seconds shows the last station to be already in transition. Transition moves forward with increasing Reynolds number until it reaches $S/r_B \approx 0.9$. It remains here between 2.8 and 5.1 seconds during which time there is a large change in free-stream Reynolds number and Mach number. At

5.4 seconds the three measuring stations between $S/r_B = 0.6$ to 0.9 appear to be in transition and at 5.6 seconds these three stations all show fully turbulent flow, leaving only the first measuring station ($S/r_B = 0.416$) in laminar flow. The Reynolds numbers of transition during the flight are as follows:

Figure	t, sec	M_∞	$R_{\infty,1}$	$(S/r_B)_T$	$(R_{\infty,1})_T$	$R_{\theta,T}$
11(a)	2.2	1.72	11.5×10^6	1.34 to 1.92	3.9 to 5.6×10^6	$1,250$ to $1,600$
11(a)	2.8	2.33	15.0	≈ 0.9	3.3	1,090
11(a)	3.6	2.71	16.6	≈ 0.9	3.7	1,020
11(b)	4.4	3.18	18.3	≈ 0.9	4.1	1,030
11(c)	4.8	4.25	23.6	≈ 0.9	5.3	1,080
11(d)	5.1	5.14	27.6	≈ 0.9	6.3	1,050
11(d)	5.4	6.10	31.0	0.416 to 0.62	3.2 to 7.1	350 to 630
11(e)	5.6	6.68	32.6	0.416 to 0.62	3.4 to 5.1	350 to 620

^aTransition occurs between two stations given.

The values of R_θ (local Reynolds number based on laminar boundary-layer momentum thickness) were calculated by using the pressure distribution of figure 9, which was assumed to be invariant ($p_l/p_{t,2} = \text{Constant}$) with Mach number, and the method of reference 12.

Comparison With Previous Investigations

A direct comparison with recent flight-test results obtained by the Langley Pilotless Aircraft Research Division (refs. 1 to 4) to show the effect of shape or roughness is difficult, since both shape and roughness are different from previous tests; however, some qualitative observations may be made.

References 1 and 2 present data on several blunt nose shapes at free-stream Reynolds number conditions as high as 18×10^6 to 24×10^6 , based on a length of 1 foot. The surface roughness of these shapes was 25 microinches or greater. During the high Reynolds number portion of these tests, the local Reynolds numbers of transition based on calculated momentum thickness were on the order of 200 to 400 and the physical location showed little or no variation.

References 3 and 4 present data on several blunt shapes which were highly polished to a 0 to 5 microinch finish. The minimum momentum thickness Reynolds numbers of transition during these tests were of the order of 800 to 900. It is to be noted that, during the present test, as long as the free-stream Reynolds numbers based on a length of 1 foot were equal to or below the test conditions of references 1 to 4 ($R_{\infty,1} = 27 \times 10^6$ at $t = 5.1$ sec), the momentum thickness Reynolds

number of transition was slightly higher ($R_{\theta,T} \approx 1,000$) than for the superpolished nose. It appears, therefore, that for similar free-stream Reynolds test conditions the 1/10-power shape with an average roughness of 6 to 8 microinches is as good as the superpolished (0 to 5 microinches) hemispheres of references 3 and 4. The two possibilities which cannot be separated here are that either the 1/10-power shape is superior or no additional benefit was obtained by reducing the roughness of the hemispheres below about 15 microinches for the test conditions of references 3 and 4.

The rapid forward movement of transition for the present case after 5.1 seconds possibly indicates that for the given surface roughness a free-stream Reynolds number of approximately 27×10^6 , based on a length of 1 foot, is critical.

Comparison of Measured and Predicted Heating Rates

The procedure used for calculating the heating rates on the forward portion of the nose appeared to be rather conservative at the most forward measuring station. Agreement at the other forward measuring stations ranged from good to fair. One possible source of the disagreement at the most forward station is the use of the pressure distribution of figure 9, both in modifying the theory of Stine and Wanlass (ref. 9) and in calculating the values of T_2 . Another source of error lies in the estimate of h_t . It is apparent that a lower value of h_t would result in better agreement in the present case.

On the rearward portion of the nose the theory of reference 11 for cones in turbulent flow, used with local conditions calculated from a Newtonian pressure distribution, appeared to be adequate for calculating turbulent heating rates when the measuring stations were clearly in turbulent flow as opposed to transitional flow.

Figure 10 presents a comparison of the variation of h_l/h_t as obtained from the theory of reference 9 with the laminar data of the present test. The heating at the most forward stations is considerably lower than theory. The figure shows clearly that transition for most of the test is in the region of S/r_B between 0.80 and 0.90.

The hemispherical shape is the most commonly used shape for which high heating rates are encountered. It is of interest, therefore, to compare the local heating rates on the 1/10-power shape with those on the hemisphere. Figure 12 presents a comparison of the experimental and calculated heating rates for the 1/10-power shape with theoretical values for a hemisphere of 6-inch diameter for Mach numbers of 5.14 and 6.68. The theory of Stine and Wanlass (ref. 9) was used to calculate the laminar

values for both the hemisphere and the 1/10-power nose. The theory of Van Driest (ref. 13) was used to calculate the turbulent values on the hemisphere. For a Mach number of 5.14, where laminar flow exists to a value of S/r_B of about 0.9, the heating rates to the 1/10-power nose are higher only at $S/r_B = 0.6$, the difference here being on the order of 10 percent. The much lower heating rates on the 1/10-power nose at $S/r_B = 0.416$ and forward of this point (note calculated values for $x^{1/10}$) indicates that the present shape is superior to the hemisphere for some applications.

This superiority evidently exists for the turbulent case also as shown in figure 12(b). The turbulent rates for the 1/10-power nose are considerably lower than the theoretical rates for the hemisphere. It should be noted that the turbulent rates behind the shoulder of the 1/10-power nose were well predicted by the theory but that those on the face were not.

CONCLUDING REMARKS

A 1/10-power nose has been flight tested at Mach numbers up to 6.7 and free-stream Reynolds numbers based on diameter of 16×10^6 . Measurements of aerodynamic heat transfer were made and conditions for transition determined. Observations were made from the test data and comparisons were made with data from previous tests. Laminar flow was obtained to local Reynolds numbers of about 1,250 to 1,600 based on calculated laminar boundary-layer momentum thickness. Laminar flow was maintained above a momentum thickness Reynolds number value of about 1,000 as long as the free-stream Reynolds number based on a length of 1 foot was less than 27×10^6 . The momentum thickness Reynolds number of transition of 1,000 was slightly higher than that obtained previously under similar test conditions for more highly polished hemispheres. At Reynolds numbers of 32×10^6 , based on a length of 1 foot, the momentum thickness Reynolds number of transition dropped as low as 350 to 600.

Langley Aeronautical Laboratory,
National Advisory Committee for Aeronautics,
Langley Field, Va., April 30, 1957.

REFERENCES

1. Chauvin, Leo T., and Speegle, Katherine C.: Boundary-Layer-Transition and Heat-Transfer Measurements From Flight Tests of Blunt and Sharp 50° Cones at Mach Numbers From 1.7 to 4.7. NACA RM L57D04, 1957.
2. Garland, Benjamine J., and Chauvin, Leo T.: Measurements of Heat-Transfer and Boundary-Layer Transition on an 8-Inch-Diameter Hemisphere-Cylinder in Free Flight for a Mach Number Range of 2.0 to 3.88. NACA RM L57D04a, 1957.
3. Buglia, James J.: Heat Transfer and Boundary-Layer Transition on a Highly Polished Hemisphere-Cone in Free Flight at Mach Numbers Up to 3.14 and Reynolds Numbers Up to 24×10^6 . NACA RM L57D05, 1957.
4. Hall, James R., Speegle, Katherine C., and Piland, Robert O.: Preliminary Results From a Free-Flight Investigation of Boundary-Layer Transition and Heat Transfer on a Highly Polished 8-Inch Diameter Hemisphere-Cylinder at Mach Numbers Up to 3 and Reynolds Numbers Based on a Length of 1 Foot Up to 17.7×10^6 . NACA RM L57D18c, 1957.
5. Rumsey, Charles B., and Lee, Dorothy B.: Measurements of Aerodynamic Heat Transfer and Boundary-Layer Transition on a 15° Cone in Free Flight at Supersonic Mach Numbers Up to 5.2. NACA RM L56F26, 1956.
6. Piland, Robert O., Collie, Katherine A., and Stoney, William E.: Turbulent and Laminar Heat-Transfer Measurements on a 1/6-Scale NACA RM-10 Missile in Free Flight to a Mach Number of 4.2 and to a Wall Temperature of 1400° R. NACA RM L56C05, 1956.
7. Ames Research Staff: Equations, Tables, and Charts for Compressible Flow. NACA Rep. 1135, 1953. (Supersedes NACA TN 1428.)
8. Sibulkin, M.: Heat Transfer Near the Forward Stagnation Point of a Body of Revolution. Jour. Aero. Sci. (Readers' Forum), vol. 19, no. 8, Aug. 1952, pp. 570-571.
9. Stine, Howard A., and Wanlass, Kent: Theoretical and Experimental Investigation of Aerodynamic-Heating and Isothermal Heat-Transfer Parameters on a Hemispherical Nose With Laminar Boundary Layer at Supersonic Mach Numbers. NACA TN 3344, 1954.
10. Van Driest, E. R.: Investigation of Laminar Boundary Layer in Compressible Fluids Using the Crocco Method. NACA TN 2597, 1952.
11. Van Driest, E. R.: Turbulent Boundary Layer on a Cone in a Supersonic Flow at Zero Angle of Attack. Jour. Aero. Sci., vol. 19, no. 1, Jan. 1952, pp. 55-57, 72.

12. Anon.: X-17 Re-Entry Test Vehicle - R-1 Final Flight Report. Rep. No. MSD-1834 (Contract No. AF 04(645)-7), Lockheed Aircraft Corp., July 17, 1956.
13. Van Driest, E. R.: The Problem of Aerodynamic Heating. Aero. Eng. Rev., vol. 15, no. 10, Oct. 1956, pp. 26-41.

~~CONFIDENTIAL~~

TABLE I
SKIN THICKNESSES AND THERMOCOUPLE LOCATIONS

Thermocouple	S/r_B	Skin thickness, in.
1	0.416	0.047
2	.611	.047
3	.742	.044
4	.910	.047
5	1.340	.037
6	1.920	.0300

~~CONFIDENTIAL~~

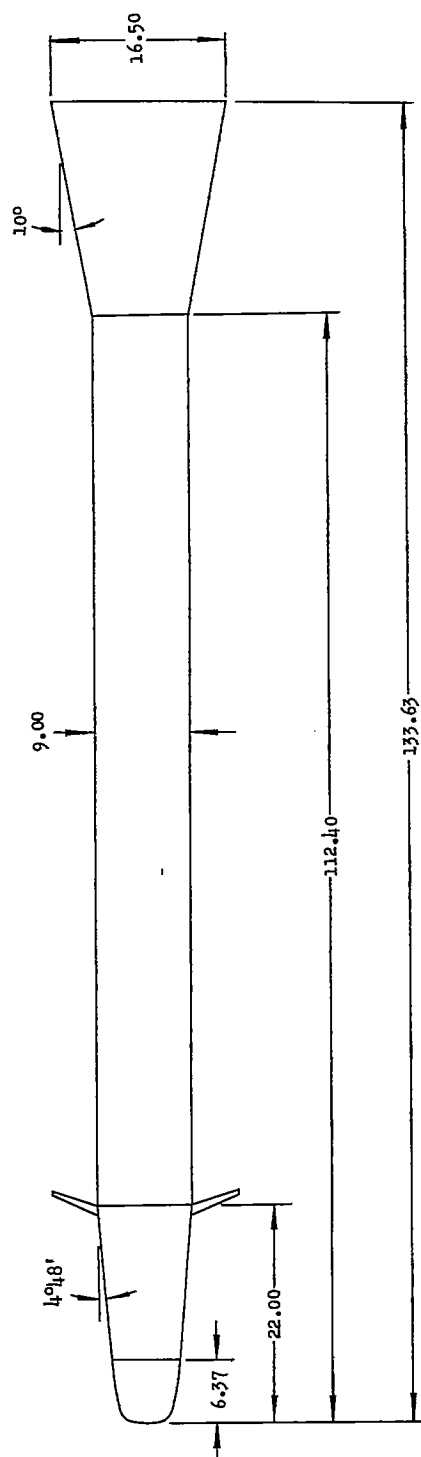
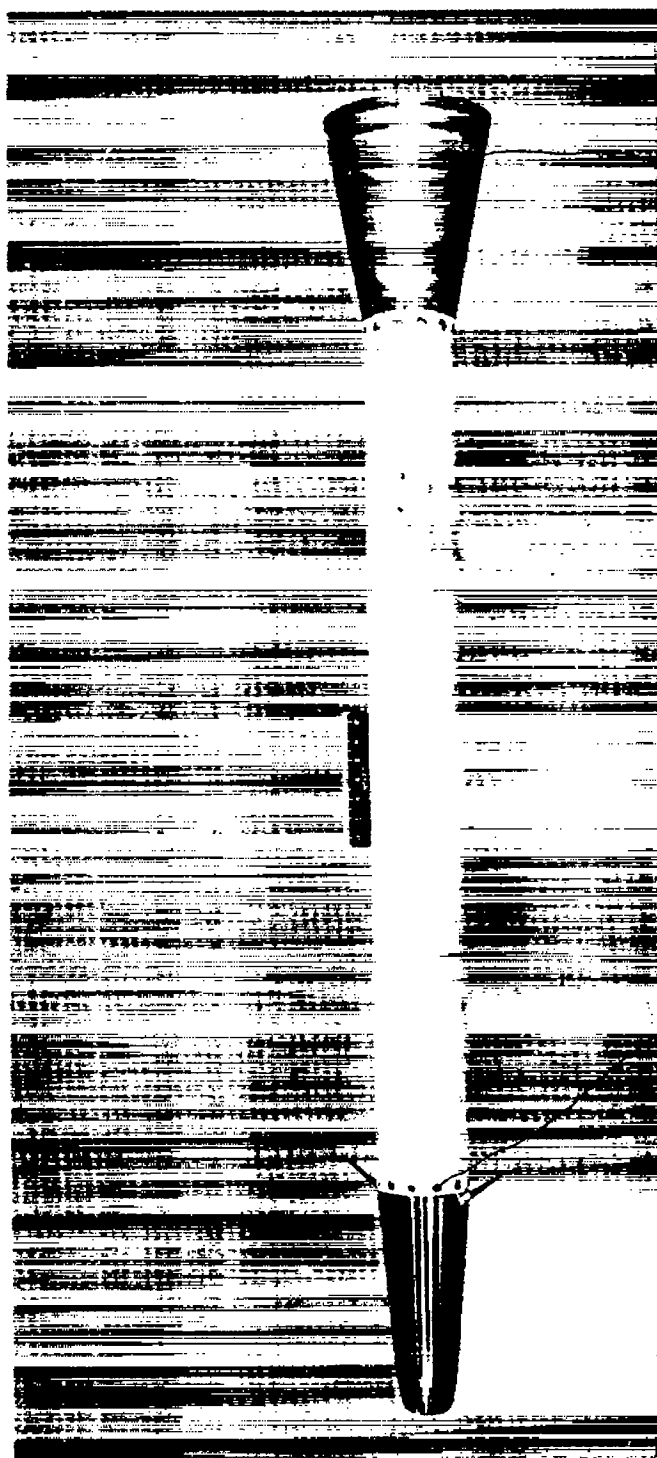


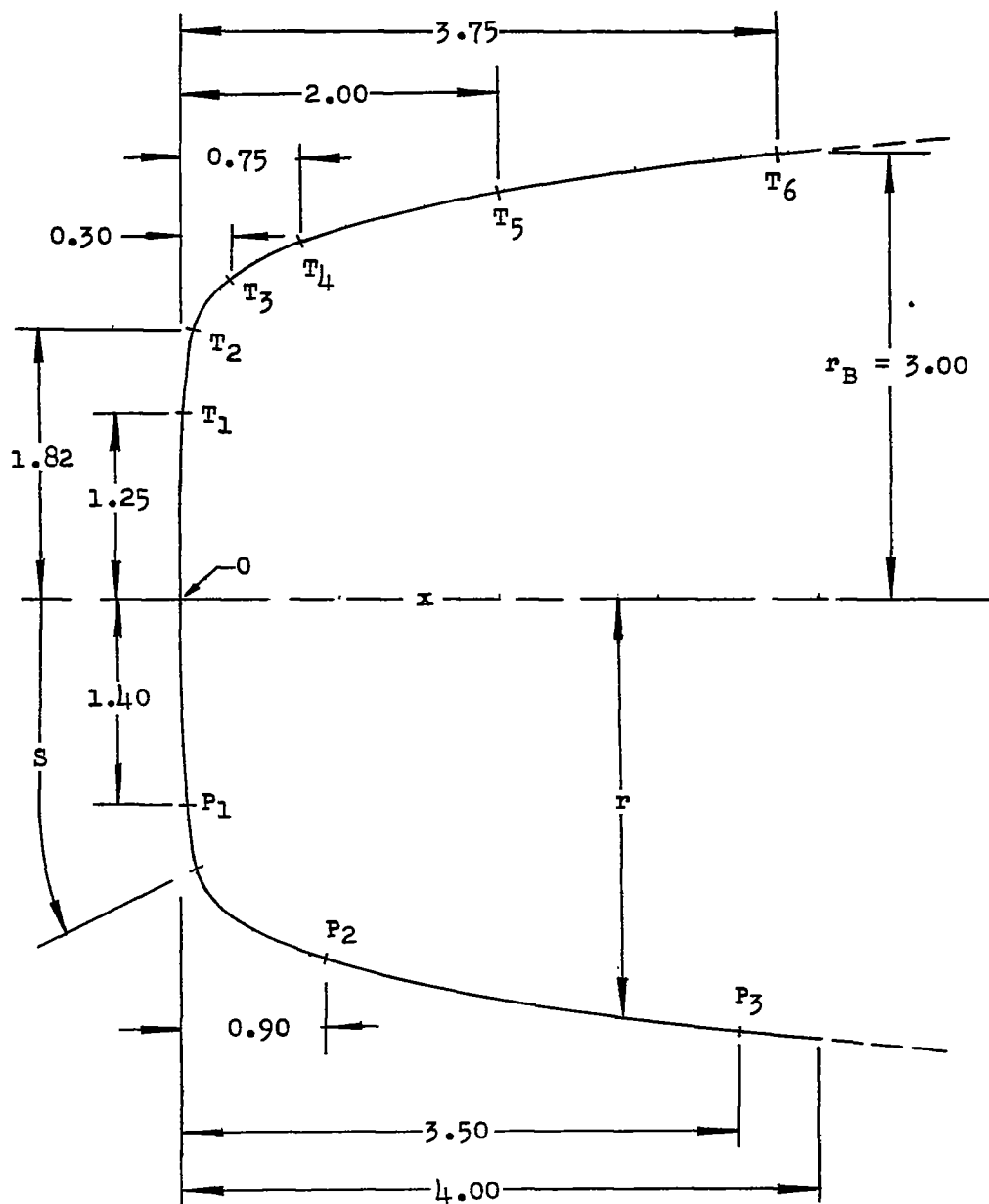
Figure 1.- General arrangement of model. All dimensions are in inches.

~~CONFIDENTIAL~~

L-97222.1

Figure 2.- Photograph of model.

~~CONFIDENTIAL~~



Equation for test nose

$$r/r_B = 0.79750x^{1/10} + 0.02078x$$

Figure 3.- Sketch of test nose. All dimensions are in inches.



Figure 4.- Photograph of test nose. L-97221

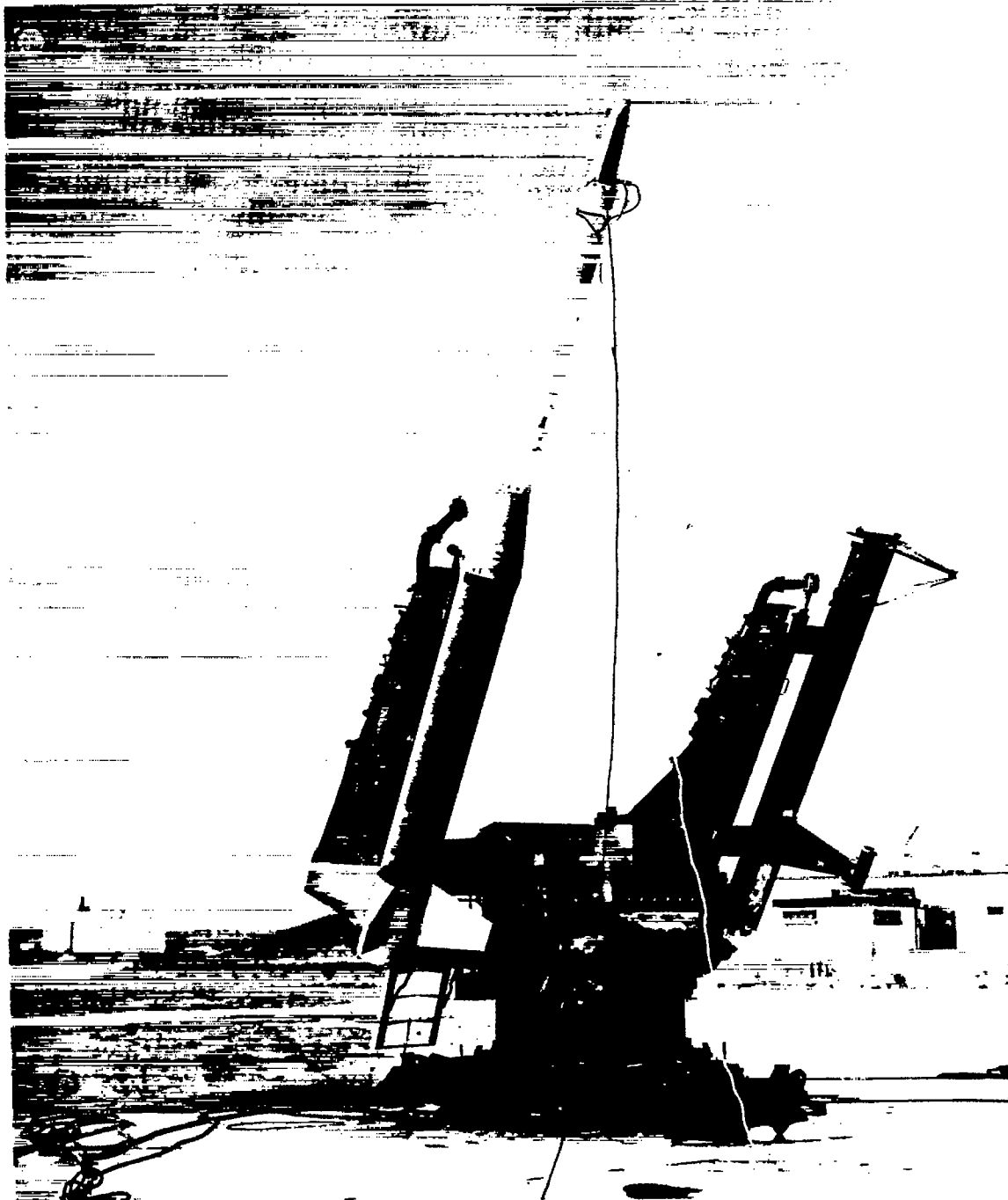
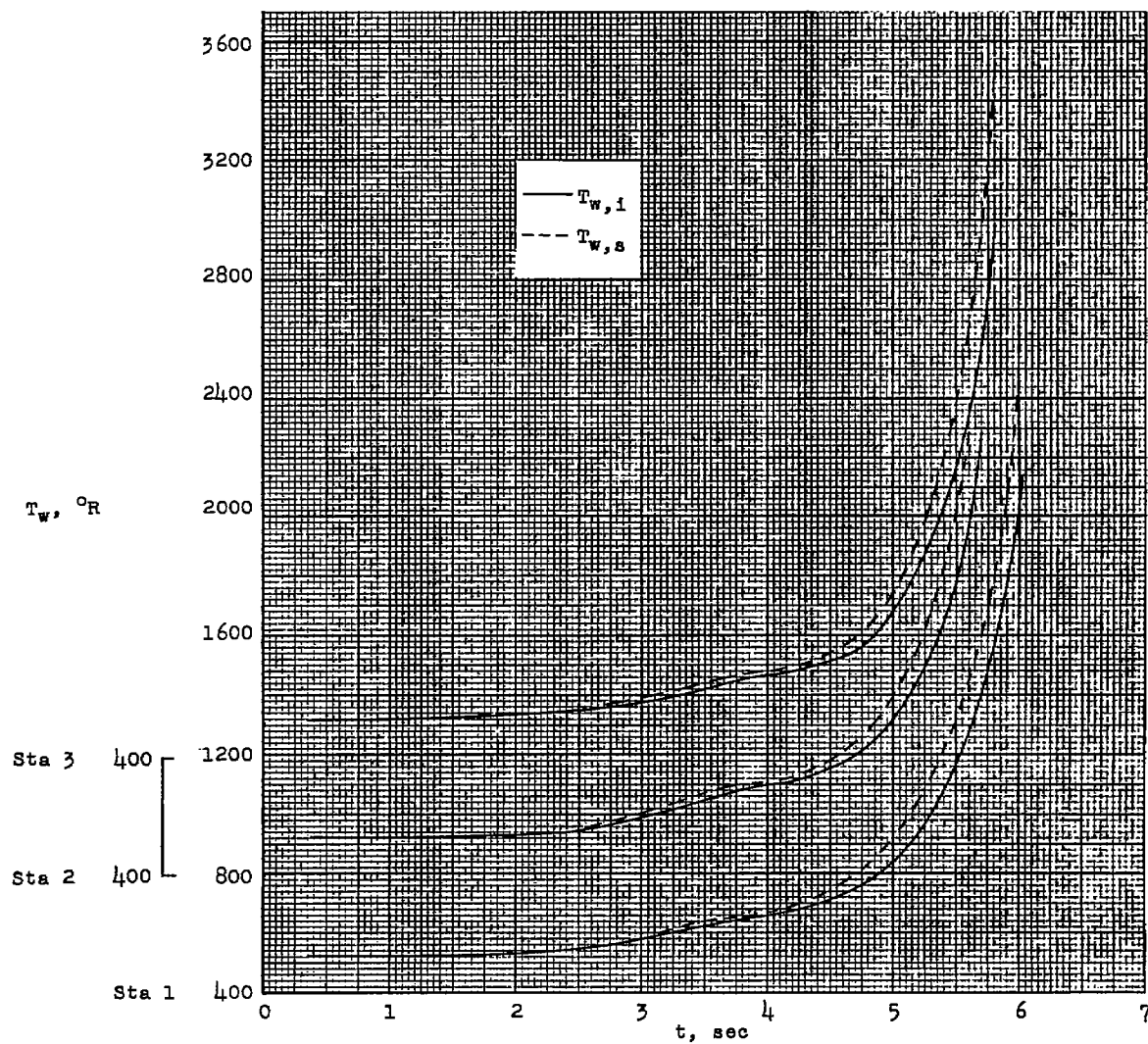
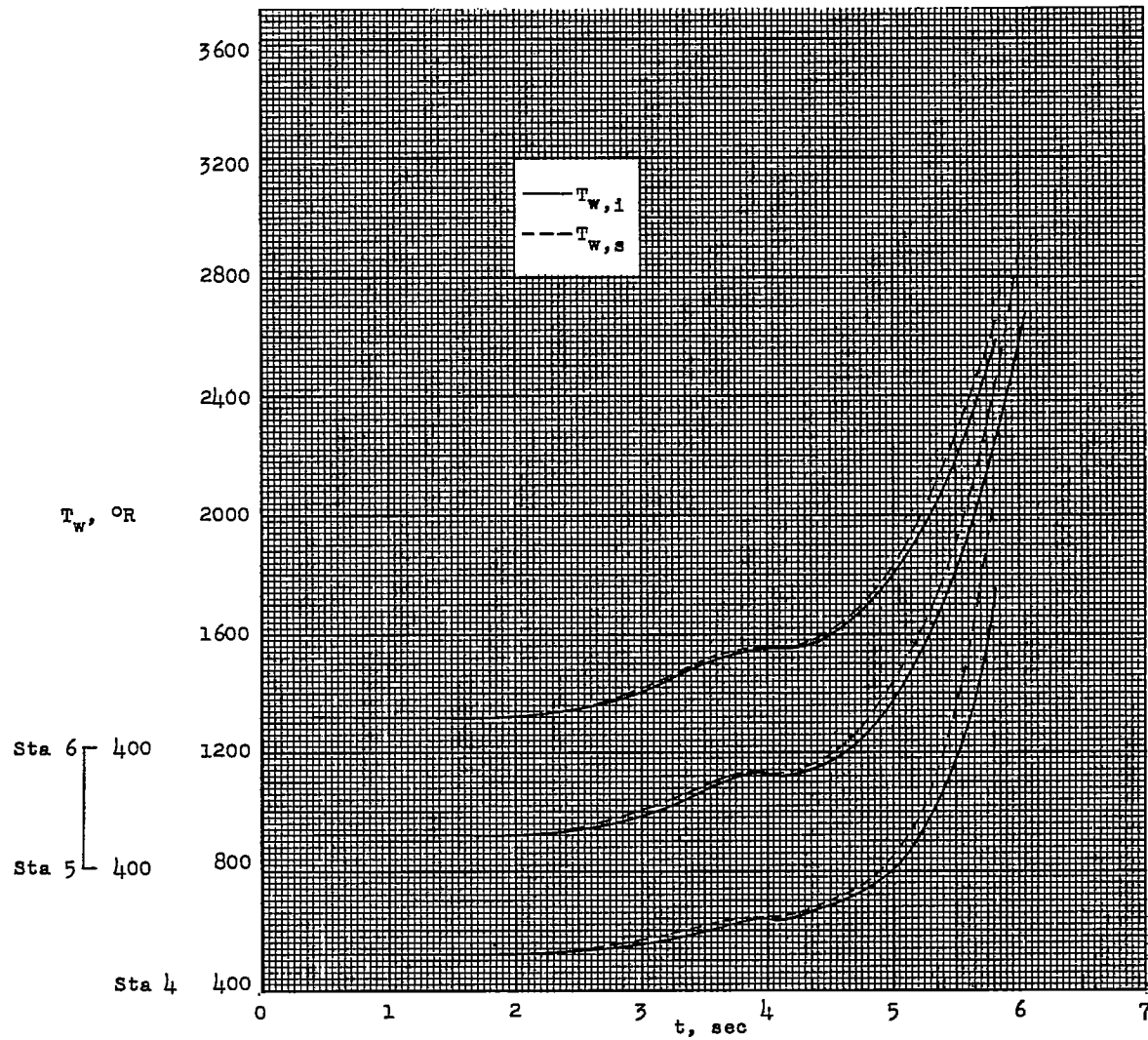


Figure 5.- Photograph of model-booster combination on launcher. L-97223.1



(a) Stations 1, 2, and 3.

Figure 6.- Variation of skin temperatures with flight time.



(b) Stations 4, 5, and 6.

Figure 6.- Concluded.

CONFIDENTIAL

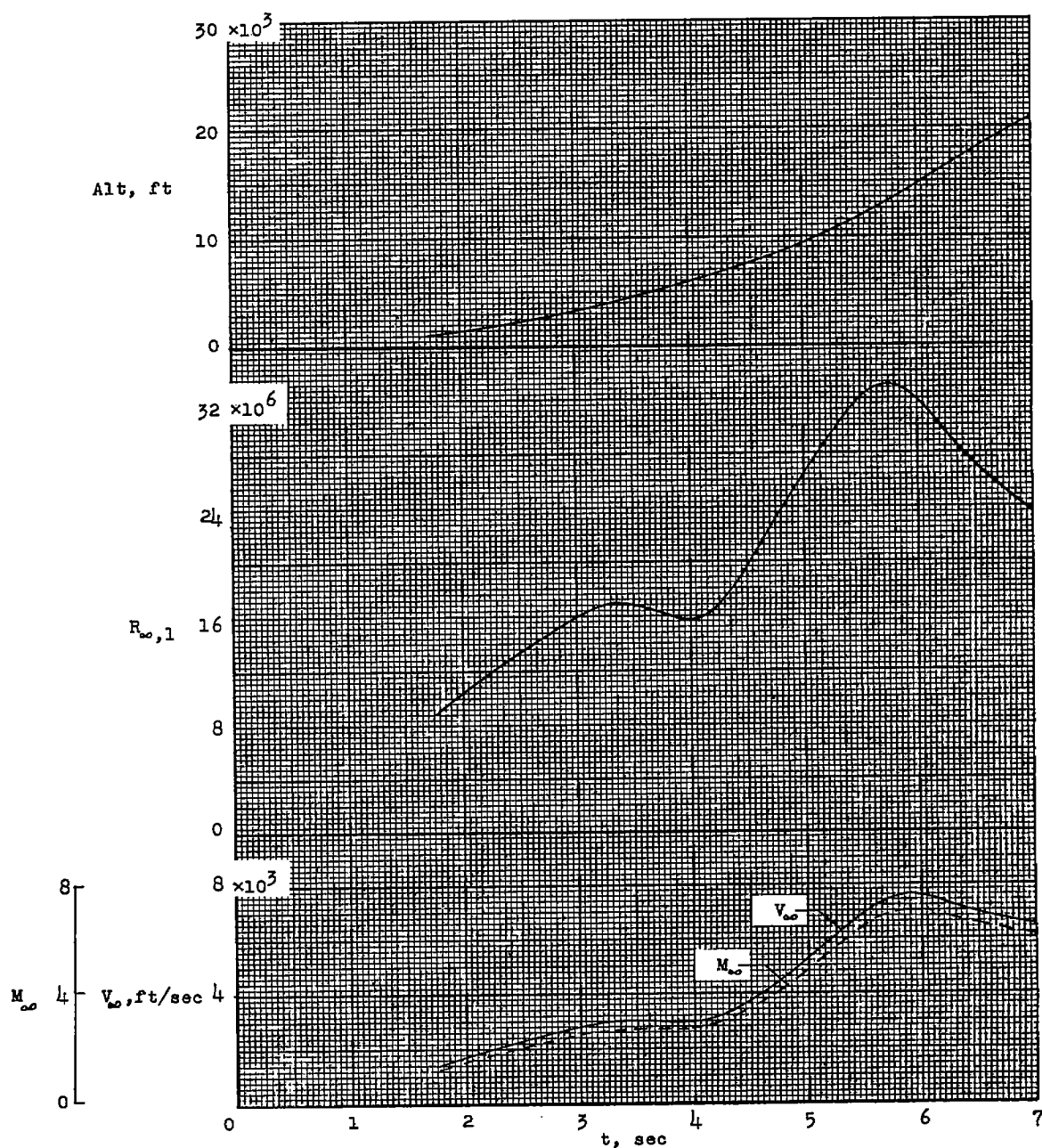


Figure 7.- Variation of model velocity, Mach number, Reynolds number, and altitude with flight time.

CONFIDENTIAL

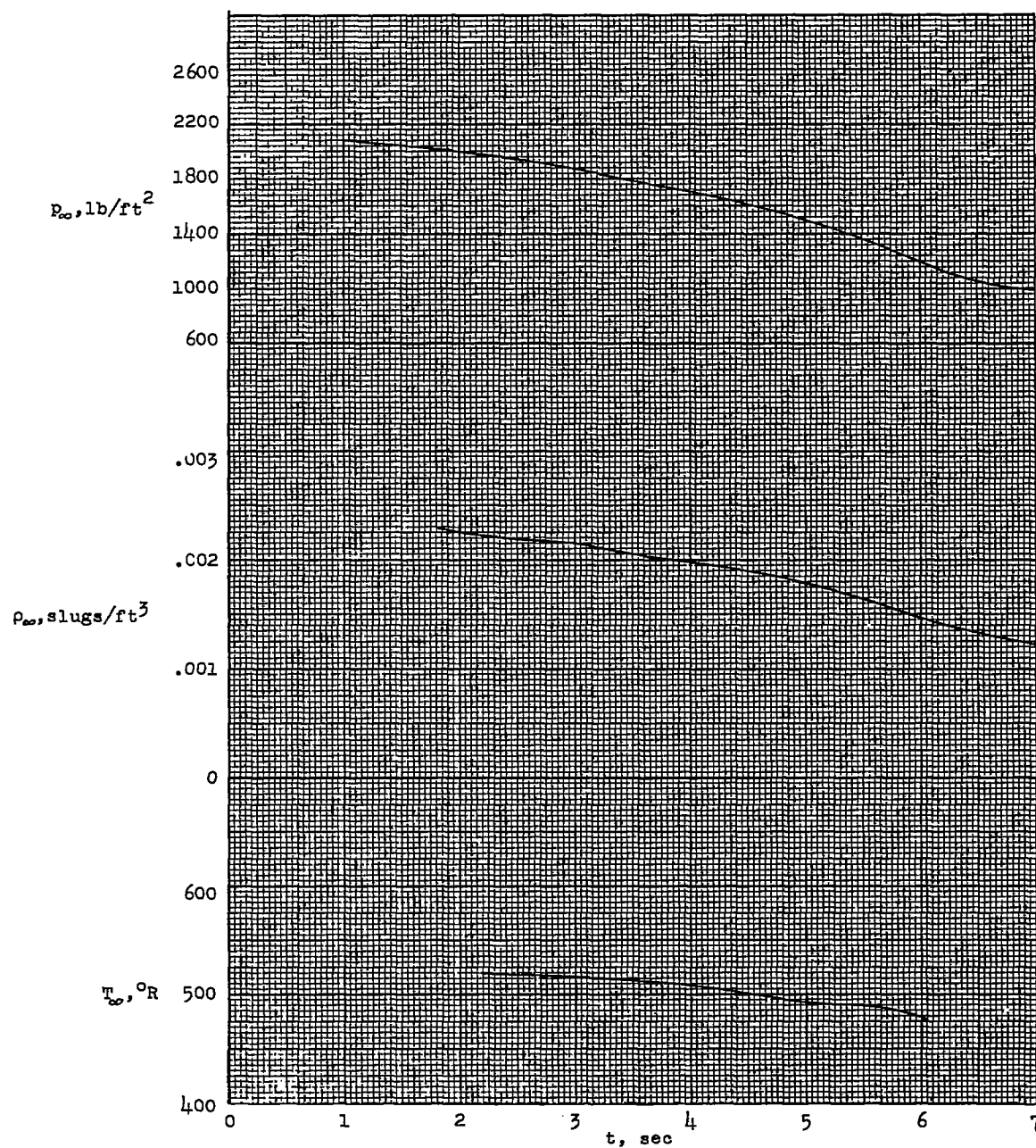


Figure 8.- Variation of static density, pressure, and temperature with flight time.

CONFIDENTIAL

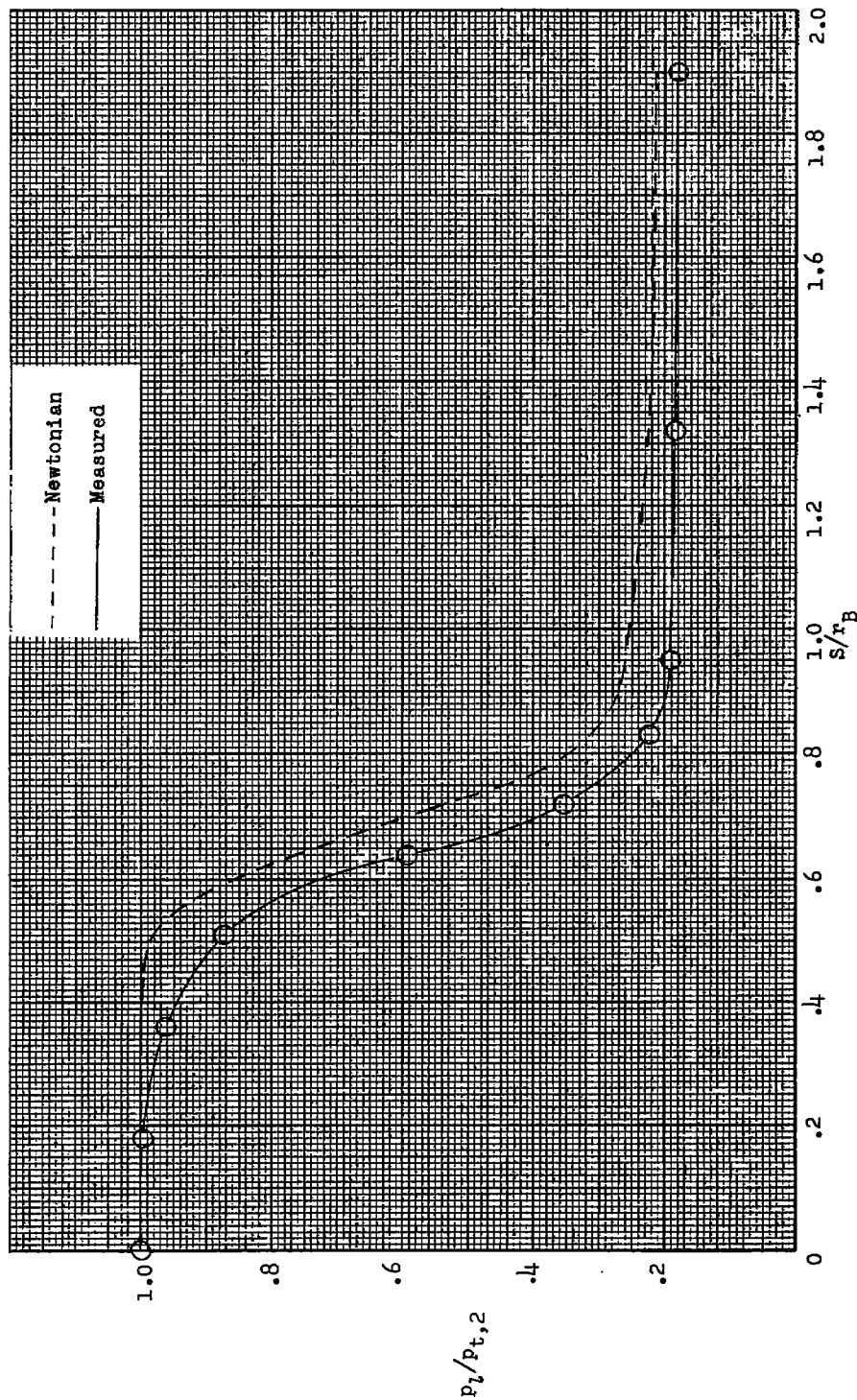


Figure 9.- Pressure distribution for 1/10-power nose shape measured in the preflight jet of Langley Pilotless Aircraft Research Station at Wallops Island, Va., and Newtonian theory for a Mach number of 2.

CONFIDENTIAL

CONFIDENTIAL

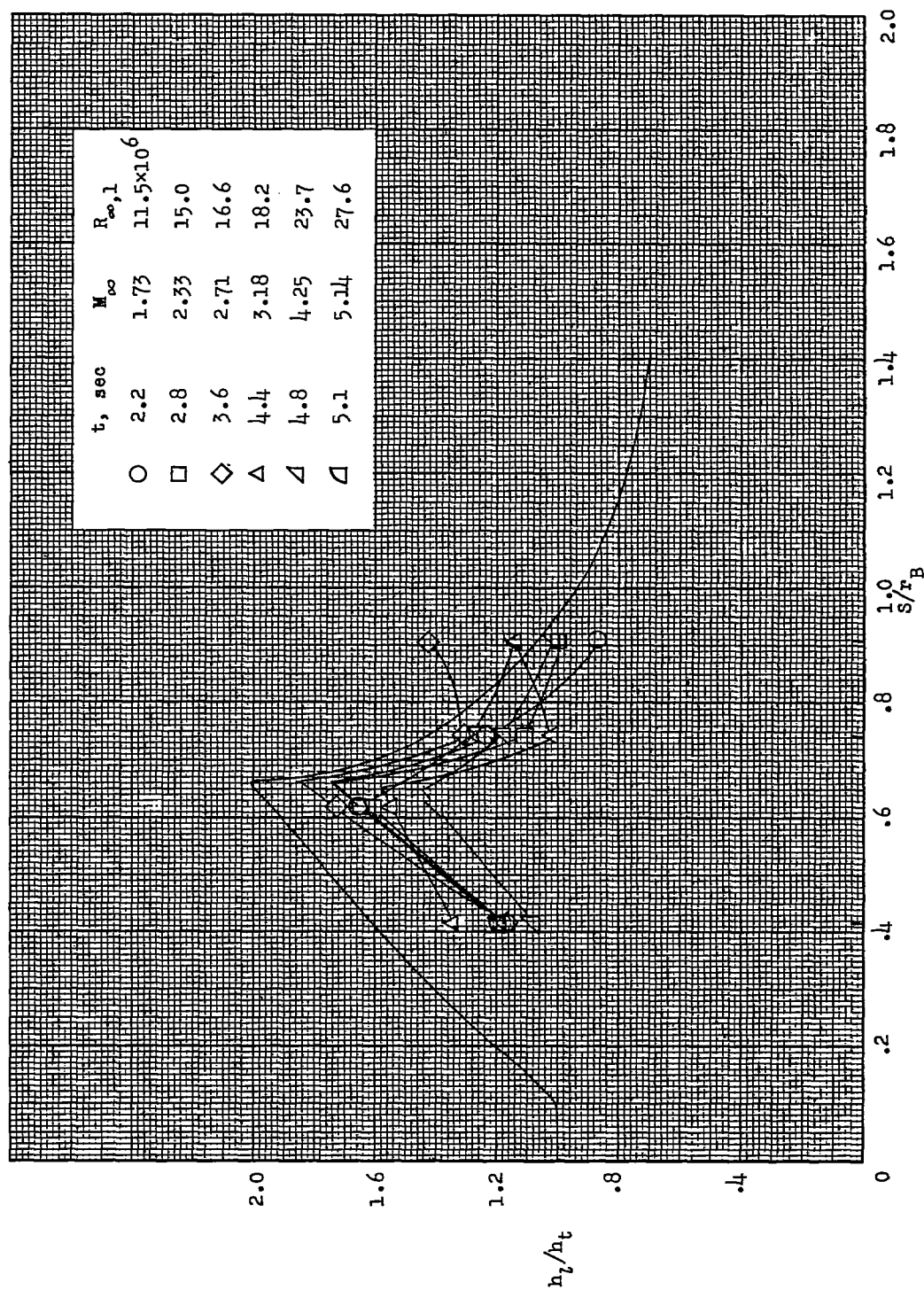
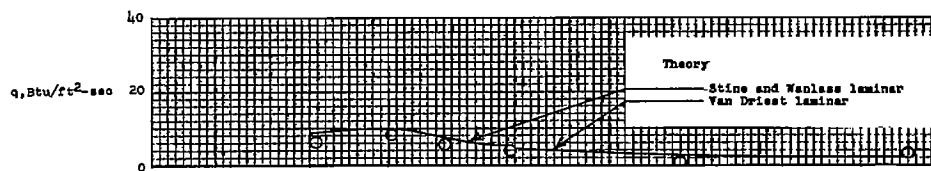
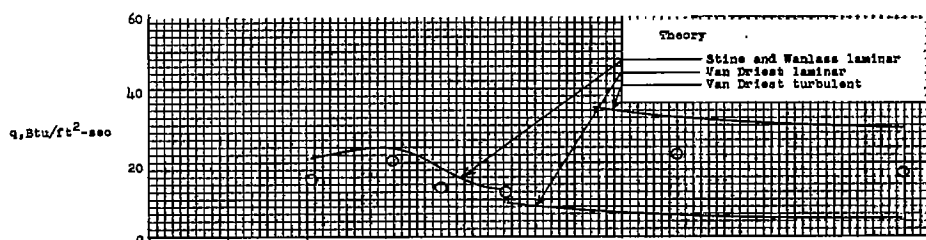


Figure 10.- Theoretical and experimental distributions of heat-transfer-coefficient ratios at various flight conditions.

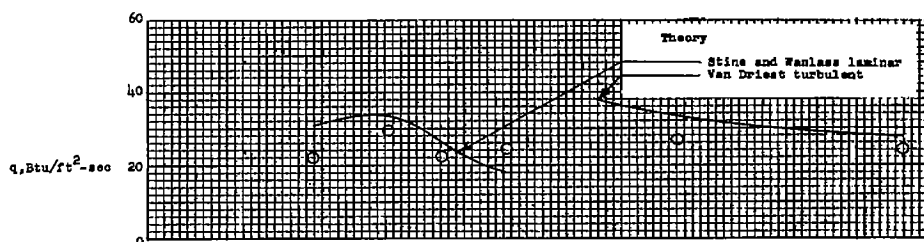
CONFIDENTIAL



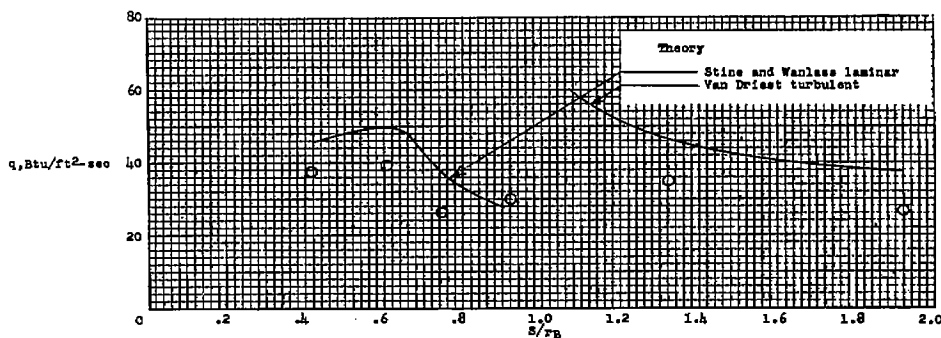
(a) $t = 2.2$ seconds; $M_\infty = 1.73$; $R_{\infty,1} = 11.5 \times 10^6$.



(b) $t = 2.8$ seconds; $M_\infty = 2.33$; $R_{\infty,1} = 15.0 \times 10^6$.

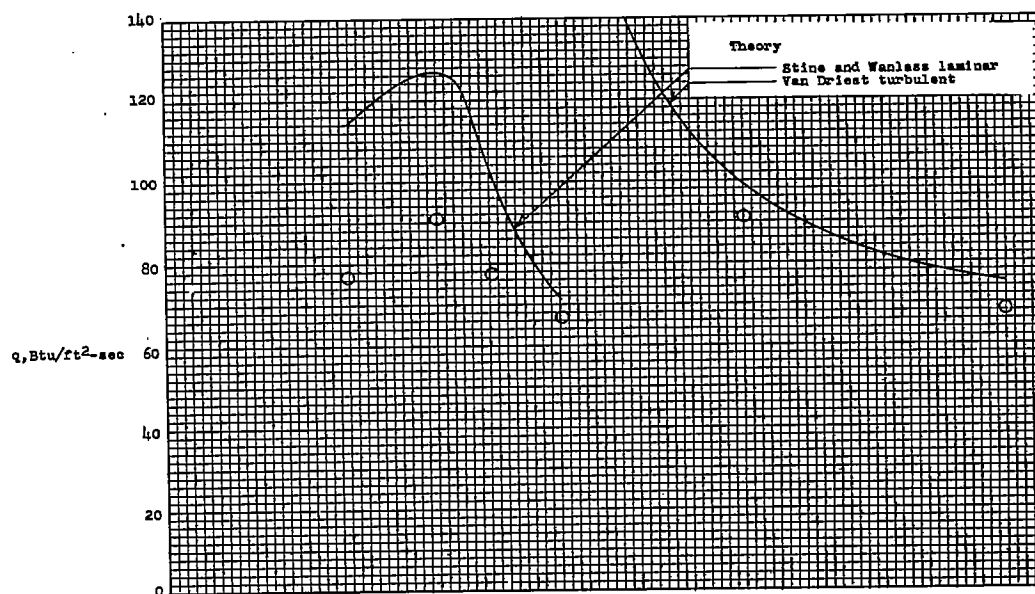


(c) $t = 3.6$ seconds; $M_\infty = 2.71$; $R_{\infty,1} = 16.6 \times 10^6$.

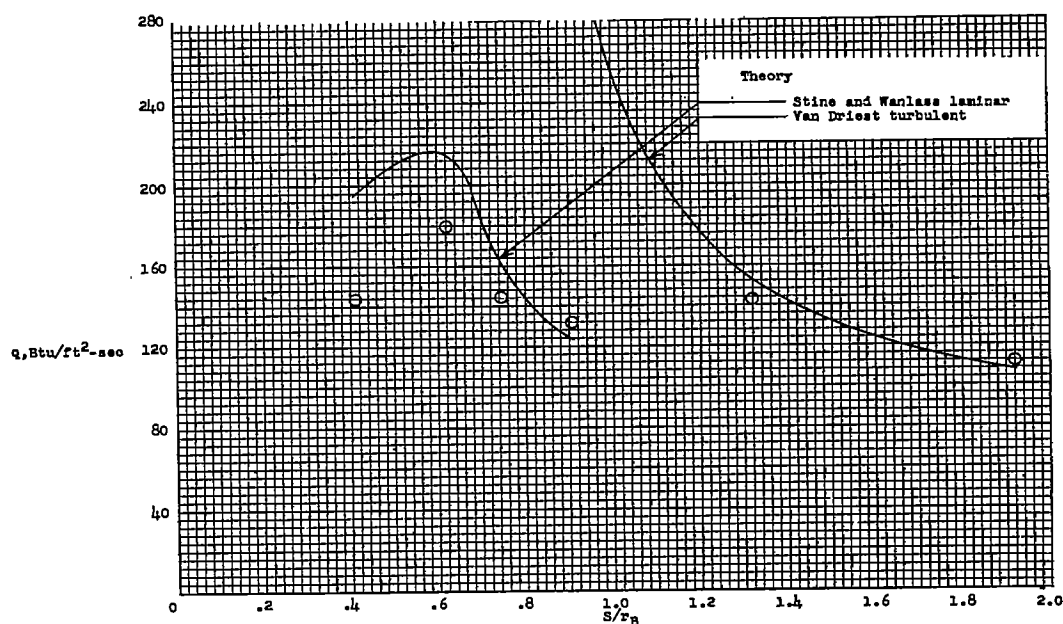


(d) $t = 4.4$ seconds; $M_\infty = 3.18$; $R_{\infty,1} = 18.3 \times 10^6$.

Figure 11.- Calculated and experimental distributions of heating rates at various flight conditions.

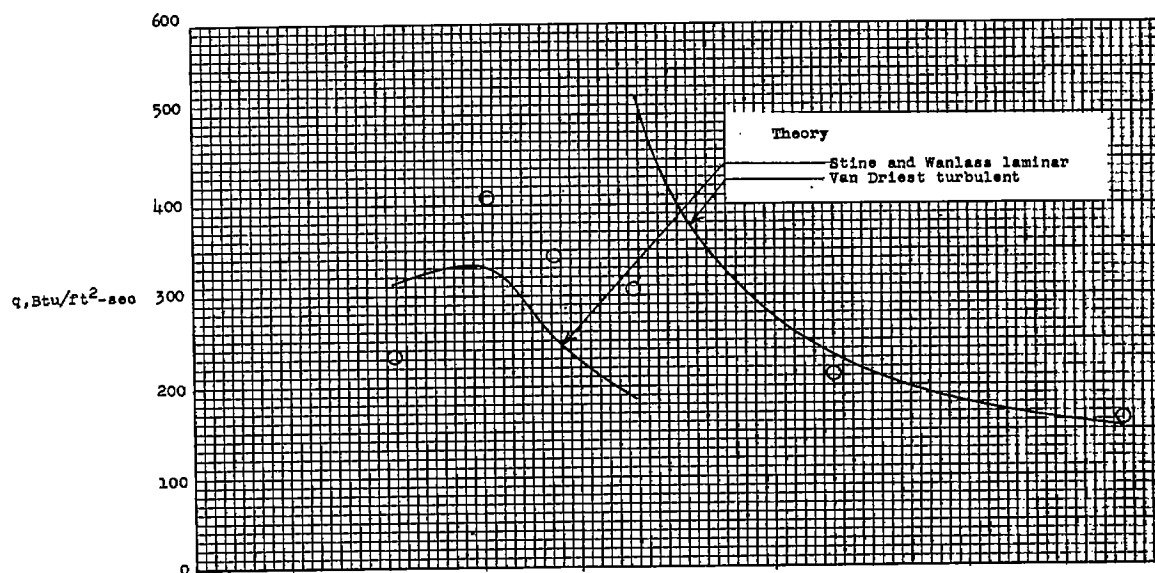


(e) $t = 4.8$ seconds; $M_\infty = 4.25$; $R_{\infty,1} = 23.7 \times 10^6$.

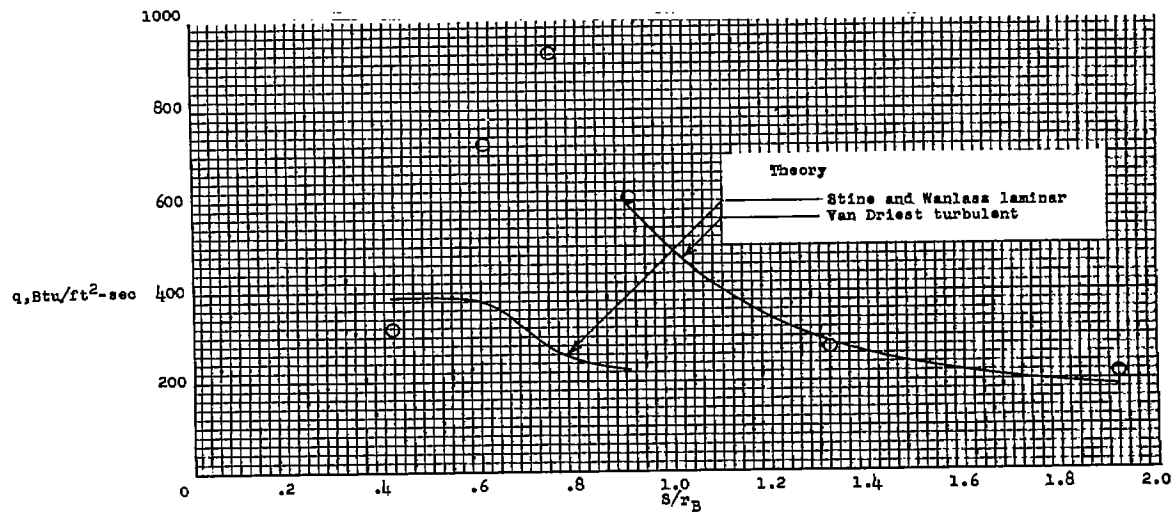


(f) $t = 5.1$ seconds; $M_\infty = 5.14$; $R_{\infty,1} = 23.7 \times 10^6$.

Figure 11.- Continued.



(g) $t = 5.4$ seconds; $M_\infty = 6.1$; $R_{\infty,1} = 31.0 \times 10^6$.



(h) $t = 5.6$ seconds; $M_\infty = 6.68$; $R_{\infty,1} = 32.6 \times 10^6$.

Figure 11.- Concluded.

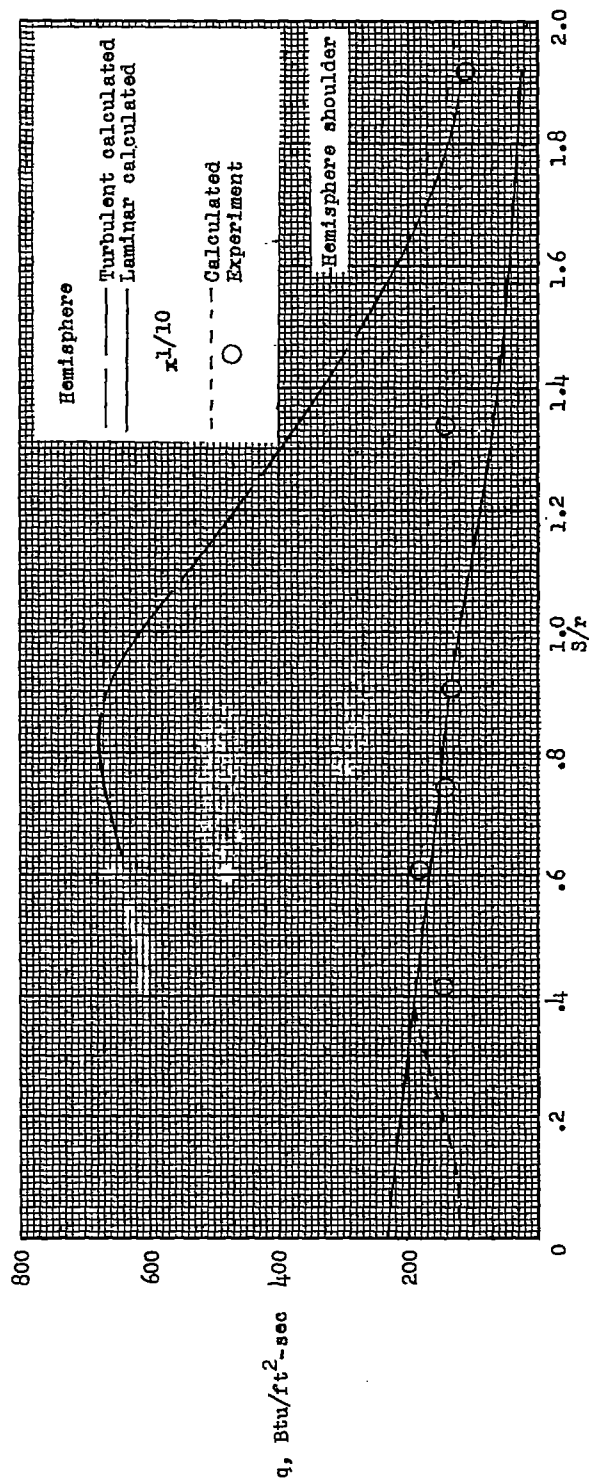
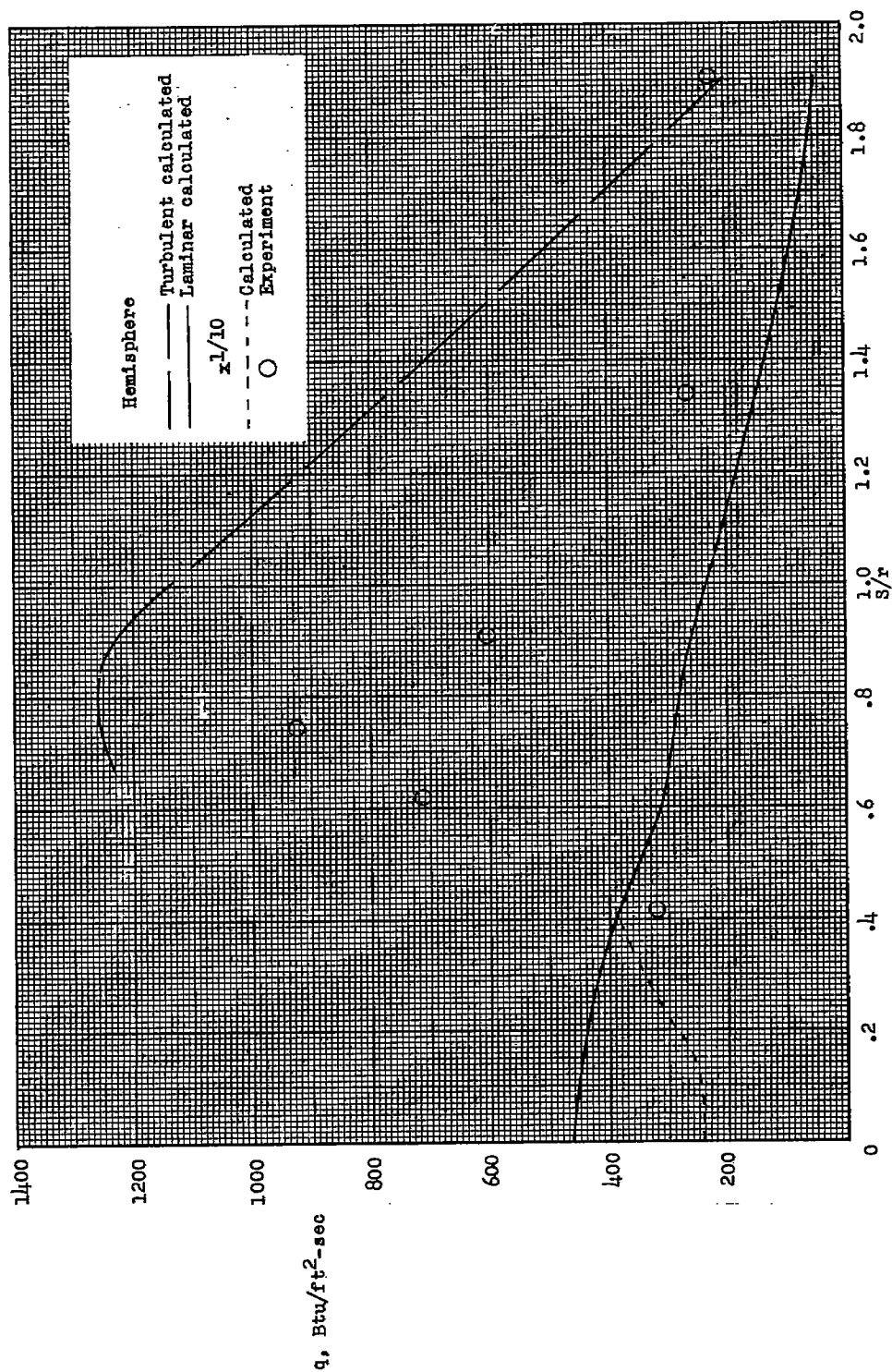
(a) $M = 5.14$.

Figure 12.- Comparison of local heating rates on 1/10-power nose shape and hemisphere.



(b) $M = 6.68$.

Figure 12.- Concluded.